RESEARCH PAPER

Enhancing Epoxy's Thermal and Mechanical Properties in a Multi-Phase Nanocomposite (EP/PVAc/CT-CS/CF)

Neda Alimirzaie [1], and Masood Hamadanian [1,2]*

[1] *Institute of Nano Science and Nano Technology, University of Kashan, Islamic Republic of Iran*

[2] *Department of Physical Chemistry, Faculty of Chemistry, University of Kashan, Islamic Republic of Iran*

ARTICLE INFO

ABSTRACT

Despite the numerous benefits of thermoset epoxy resin, such as its high thermal and chemical stability and excellent adhesion, its use is limited due to its fragile and rigid structure, low crack initiation, and potential loss of integrity from damage. To address these limitations, various types of fillers, such as fiber, particle, and crystal filaments, have been incorporated into the epoxy matrix. The focus of this study is on the synthesis of $CaTiO_3$-Ca_2SiO_4 nanoparticles through the sol-gel method and their incorporation into the epoxy matrix using the ultrasonic method, along with polyvinyl acetate (PVAc) and carbon fiber (CF). These ingredients' impact on the epoxy resin's mechanical behavior and the optimum weight percentages were evaluated using response surface methodology-central composite design (RSM/CCD). The combination of nanoparticles and carbon fibers had a synergistic effect on the overall stress of the epoxy resin, resulting in a significant increase (236.7% and 188.9%, respectively) compared to pure epoxy and epoxy with PVAc.

INTRODUCTION

Fiber-reinforced polymer (FRP) composites are heterogeneous and anisotropic materials that do not exhibit plastic deformation. FRP composites are typically utilized in various industries such as transportation, automobile, aerospace, energy storage devices, and electronics due to high strength- o-weight ratio, stiffness, good thermal insulation, anti-corrosion feature, resistance to wear, high fracture toughness, and fatigue resistance. [1, 2]. FRP composites are classified into two groups: carbon fiber-reinforced polymer (CFRP) and glass fiber-reinforced polymer (GFRP) groups.

Epoxy resin is a thermosetting resin commonly used in FRP composites due to its high thermal and chemical stability and excellent adhesion to various substrates [3]. However, its structure is brittle and rigid, It has low crack resistance, and it tends to lose its integrity when damaged. These deficiencies have limited its use as an adhesive or composite. [4, 5].

various types of fillers, such as fiber, particle, and crystal filaments (whiskers), have been used in the epoxy matrix to reduce its restriction [1]. In recent years, the utilization of polymers along with nanoparticles to improve the mechanical properties of polymer nanocomposites has been concerned. The incorporation of different nanofillers such as Carbon black nanoparticle [6],

* *Corresponding Author Email: hamadani@kashanu.ac.ir*

montmorillonite [7], graphene oxide [8] , TiO_2/ hallosyte [9], organoclay [10], sodium silicate [11, 12], Carbon nanotube[13, 14], and $CaSiO_3$ [15] has a remarkable effect On improving the modulus, mechanical properties, wear resistance, the tensile and flexural strength, crack propagation energy, oxidation, and anticorrosion properties of epoxy resin.

Incorporation of TiO_2/SiO_2 into the epoxy resin improves the elongation, yield strength, ultimate strength, and elastic modulus by 29.3, 17.72, 17.43, and 4.34%, respectively [16]. Additionally, the addition of $NiMn_2O_4$ and $CoCr_2O_4$ nanoparticles to the epoxy resin at the optimum percentages weight increases the yield and Young's modulus of EP/PU/$NiMn_2O_4$ and EP/$CoCr_2O_4$ nanocomposites [17, 18]. Furthermore, it has been reported that the nanocomposite Ag/CuO/Polyethylene Glycol in an epoxy resin matrix has higher elongation [19].

Polyvinyl acetate (PVAc) is an inexpensive and non-toxic thermoplastic polymer known as wood adhesive, synthesized from vinyl acetate monomer in the presence of vinyl alcohol. The key features of PVAc include easy handling, faster solidification, good durability, and considerable potential to improve the toughness and reduce the cure shrinkage of epoxy resin [20-22]. The incorporation of 1–1.5% nano-clay (montmorillonite) with PVAc and urea formaldehyde (UF) has been shown to increase strength resistance, shear strength, and the percentage of wood failure [23].

Another component used in FRPs includes glass, carbon, and aramid fibers [23]. The mechanical properties of epoxy matrix are improved by adding nanoclay and $CaSiO_3$ nanoparticles/E-glass fiber [24], silane-modified nanosilica particle/aramid fiber [25], and TiO_2/SiO_2/Al_2O_3 nanoparticle/glass fiber [26]. Furthermore, Carbon fibers are widely used to enhance the mechanical properties of epoxy resins due to their high specific durability, excellent elasticity modulus, and heat resistance [27]. Indeed, CFRP facilitate the transfer of stress between the weakest matrix and the strongest fibers.

Carbon fiber has also been used in epoxy/PVA/ waste glass powder composites, and the results confirmed that it increases the fatigue resistance of the epoxy resin [28]. Similarly, the residual tensile strength and modulus of epoxy resin increase with the incorporation of carbon fiber (CF) and nanoclay in its structure [29]. Additionally, the interlaminar

and intralaminar mode I fracture toughness of the carbon fiber/epoxy composite were increased by 260% and 53%, respectively, with the inclusion of nanodiamond: CNT: graphene with a 1:2:1 mass proportion [30]. By growing carbon black on the surface of carbon fiber, interlaminar shear strength (ILSS), interface shear strength tests (IFSS), and the tensile strength of epoxy nanocomposite increased compared to untreated CFs [31]. Increasing 40, 50, and 60 wt% carbon fiber to epoxy resin increased the tensile strength and Young's modulus to 844.44%, 951.11%, and 1122.22%, respectively, in Carbon fiber/glass fiber/epoxy composites [32].

Calcium silicate is a biocompatible material with poor chemical stability. To enhance the chemical stability of Calcium silicate, Titanium can be doped into its structure [33]. Earlier studies have discussed the individual impact of nanoparticles, fiber, and reinforcing polymers on enhancing the mechanical properties of epoxy resins. However, fewer studies have examined the simultaneous interaction of all three parameters in improving the mechanical behavior of epoxy resins.

This research aims to investigate the effects of three factors: $CaTiO_3$-Ca_2SiO_4 (CT-CS) nanoparticles, PVAc, and CF weight percentages on improving the mechanical properties of epoxy resin. To achieving the best results, reduce unwanted experiment, and evaluate the exact interactions among parameters, the RSM/CCD method was used (Design-Expert software version 13). Firstly, nanoparticles are synthesized using the sol-gel method, and then they are dispersed in epoxy resin using an ultrasonic probe in the presence of PVAc and CF. The chemical characterization of nanocomposite and nanoparticles was confirmed by XRD, FTIR, SEM/EDAX, and TGA analysis. Mechanical parameters, such as stress, strain, and area, were optimized and measured with a tensile test device.

MATERIALS AND METHODS
Material

The materials used are Calcium nitrate tetrahydrate ($Ca(NO_3)_2.4H_2O$) and titanium tetraisopropoxide (TTIP) as the precursors. Ammonia (25%) and Nitric acid (65%) as pH adjusters, polyvinylepyrrolidone (PVP) as the surfactant, Acetic acid, and Ethanol as the solvent were all obtained from Merck (Darmstadt, Germany). Epoxy resin and cycloaliphatic amine

as a hardener were supplied from Kumho and Kukdo chemical industry companies (Seoul, South Korea) with trade names KER 828 and KH 816, respectively. Isfahan Ab Shishe Company (Isfahan, Iran) supplied Sodium metasilicate (Na_2SiO_3), Carbon fiber from Iran composite Kavian (Tehran, Iran), and Polyvinyleacetate (PVAc) purchased from Samed Gmbh (Dresden, Germany).

Synthesis of CT-CS nanoparticles

3.95 gr Sodium metasilicate was dissolved in 50 ml of distilled water. The the pH was adjusted to 3 by adding drop by drop, of nitric acid, and afterward to 8 by adding ammonia to the solution. 1.36 gr (0.544 moles) of PVP was added to the former solution and then stirred for 60 minutes (solution A). 20 gr (84.69 mmoles) of $Ca(NO_3)_2.4H_2O$ and 1.36 gr (0.544 moles) of PVP were separately dissolved in 50 ml distilled water and stirred for 60 min (solution B). Subsequently, solution B was added to solution A, resulting in the formation of Ca_2SiO_4 sol .To prepare titanium

sol, 92 ml (1.6355 moles) of acetic acid was added into a beaker and allowed to freeze for 15 minutes. Then, 9 ml (30.98 mmoles) of TTIP and 92 ml (1.5967 moles) of ethanol were added to the former solution. Subsequently, Ca_2SiO_4 sol was added drop by drop to the Titanium solution and stirred for 1 hour. Afterward, a gel was formed and placed under aging condition overnight. The resulting powder was dried at 100°C for 24 hours and then calcined at 950°C for 2 hours was being stored for further analysis [34]. This preparation is depicted Fig. 1.

Experimental design

In this research, response surface methodology/central composite design from Design expert software (version 13) is used for modeling and statistical optimization studies of the nanocomposite. This method is used in processing the composition of nanocomposite components to determine how changes in processing conditions affect properties such as
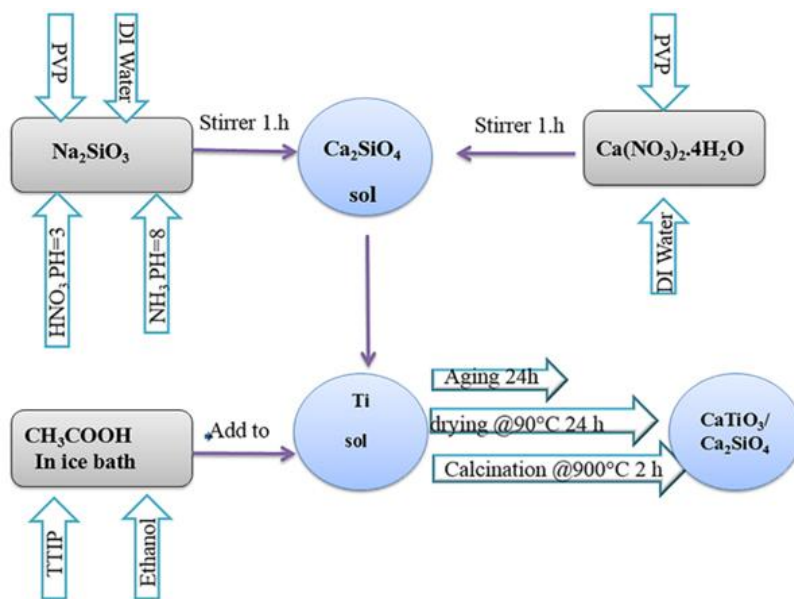
Fig. 1. Synthesis of $CaTiO_3$-Ca_2SiO_4 nanoparticles: a demonstration schematic.

Table 1. Design matrix for central composite design of EP/PVAc/CT-CS/CF nanocomposite.

variables	Units	Symbol	Low	High	-alpha	+alpha
NPs	weight %	A	0.304	1.195	0	1.5
CF	weight %	B	0.202	0.797	0	1
PVAc	weight %	C	2.81	5.189	2	6

tensile strength. Response surface methodology/ central composite design is utilized for optimizing affecting factors. Table 1 displays the design matrix for the central composite design.

Preparation of EP/PVAc/CT-CS/CF nanocomposite

Various amounts of Carbon fiber, CT-CS nanoparticles and PVAc with different weight percentages, which are calculated for 20 experiments according to Table 2, were added to EP resin and stirred for 1 h, and then sonicated to obtain a homogeneous mixture. A certain amount of hardener was added to the solution, then the mixture was poured into a silicone mold (ASTM d 638). The carbon fiber was embedded in the structure of the nanocomposite mixture inside a
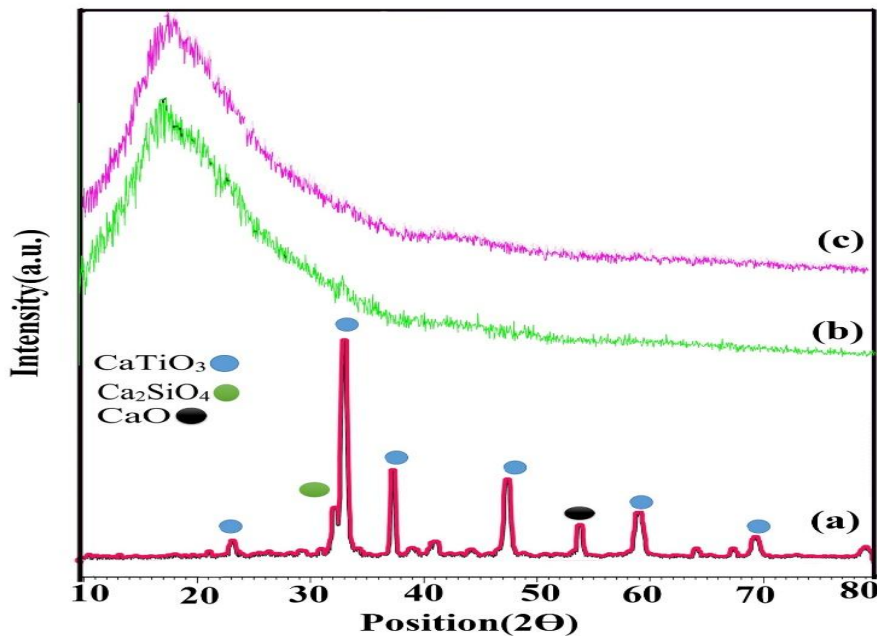
Fig. 2. The XRD patterns of $CaTiO_3$-Ca_2SiO_4 Nanoparticle (a), the optimum nanocomposite with maximum stress (b) and maximum strain (c).

Table 2. Experimental design matrix and mechanical factors of EP/PVAc/CT-CS/CF nanocomposite.

Run	Weight %			Stress (MPa)	Strain (%)	Area (J/m³)
	A (NPs)	B(CF)	C(PVAc)			
1	0.75	0	4	12.92	5.20	125.87
2	0.75	0.5	4	17.79	6.45	175.58
3	0.75	0.5	2	21.29	6.53	219.14
4	0.304	0.202	5.189	18.69	6.57	282.60
5	1.195	0.202	2.81	14.31	7.16	195.36
6	1.5	0.5	4	23.57	8. 10	336.28
7	0.75	0.5	4	20.81	6.77	202.99
8	0.75	0.5	4	23.08	7.02	255.25
9	0.75	0.5	6	24.51	7.40	313.06
10	0.304	0.797	2.81	22.07	7.76	312.14
11	1.195	0.797	2.81	31.49	6.02	465.81
12	0.304	0.797	5.189	34.45	8.06	635.03
13	0.75	0.5	4	23.69	7.22	263.60
14	0.75	1	4	39.05	6.98	499.43
15	1.2	0.202	5.189	18.64	6.98	224.49
16	0.75	0.5	4	21.06	9.74	379.27
17	0	0.5	4	14.31	7.16	195.36
18	0.75	0.5	4	20.24	7.02	219.71
19	0.304	0.202	2.81	13.54	7.02	185.65
20	1.195	0.797	5.189	29.56	6.21	513.00

silicon mold.

Characterization techniques

XRD patterns of CT-CS nanoparticles and fabricated nanocomposites were recorded in 2θ range of 10°–80° with a Philips X-pert pro-MPD model X-ray diffractometer using Cu Kα radiation (λ = 0.1540 nm) as the X-ray source. The cross-section and surface morphology of the nanocomposites were obtained using energy-dispersive X-ray detector (EDAX)-equipped scanning electron microscopy (TESCAN). FT-IR analysis was performed using a Nicolet-Impact 400D spectrophotometer. The samples were analyzed using UV-Vis diffuse reflectance spectroscopy (UV-Vis DRS) with a Shimadzu 1800 spectrometer. Thermal gravimetric analysis (TGA, BAHR STA 503 model, Germany) was used to record the materials' TGA curves. A Faratest 5

Ton (Iran) mechanical device was used for tensile testing.

RESULTS AND DISCUSSION

Nanoparticle characterization
XRD analysis

The XRD patterns of $CaTiO_3$-Ca_2SiO_4 and the optimum nanocomposite with maximum stress and maximum strain are illustrated in Fig. 2. $CaTiO_3$ nanoparticles have been observed in a diffraction pattern at 2θ (23.25(101), 32.87(002), 33.12(121), 33.36(200), 47.54(202), and 59.47(321)) with an orthorhombic phase, according to the JCPDS number (01-072-1192). Similarly, the diffraction pattern of Ca_2SiO_4 with hexagonal phase and JCPDS number (01-086-0401) has been demonstrated at 2θ (31.78(102), 33.02(110), 40.49(201), and 58.02(212)). Of course, CaO, with JCPDS number (0-0-002-1087), has been identified as an impurity
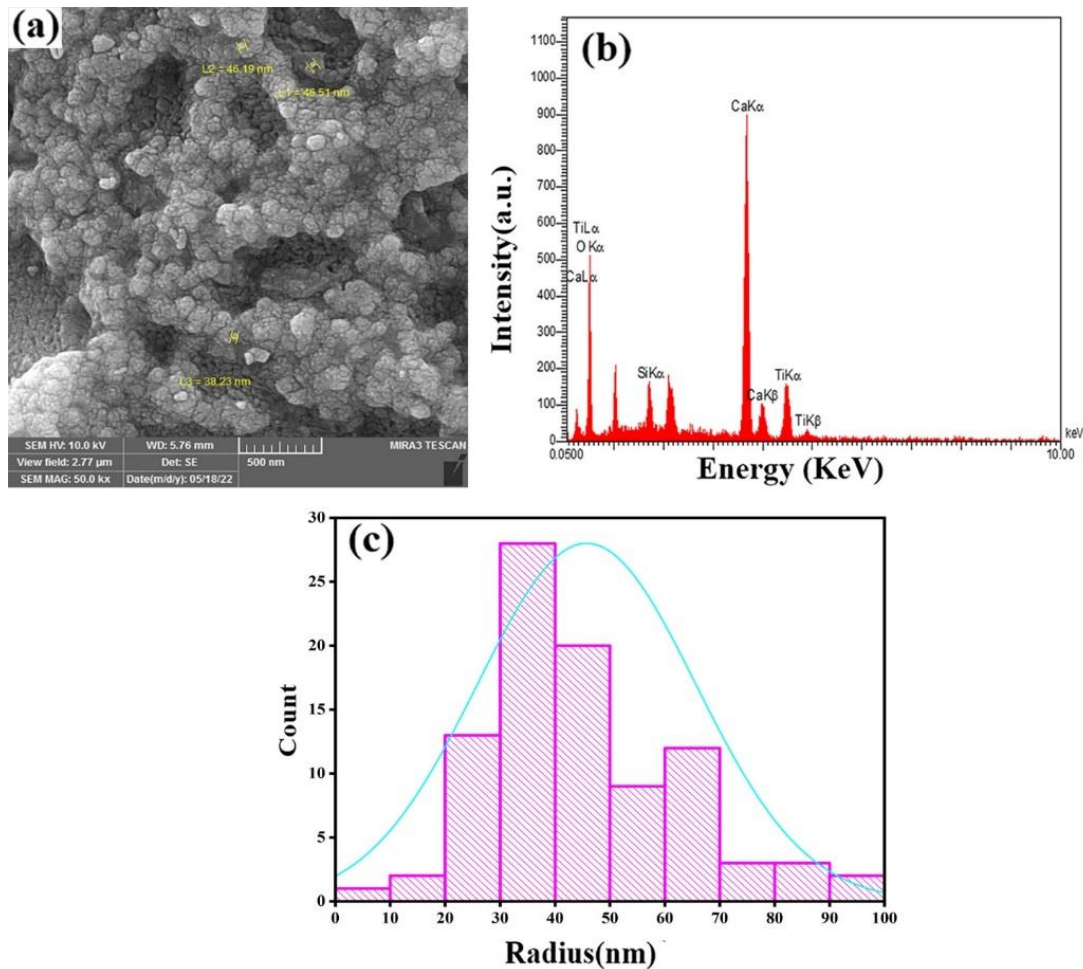
Fig. 3. SEM images (a), EDX (b), and size distribution histogram (c) of $CaTiO_3$-Ca_2SiO_4 nanoparticles.

with a cubic structure at 2θ (37.2(200), 54.23(220).

The average crystallite size of $CaTiO_3/Ca_2SiO_4$ was calculated by the Debby Scherrer formula (Eq. 1). Where D is the crystalline size, K is a constant, β is the width at half the height of the peak, λ is the wavelength of X-rays, and θ is the diffraction angle.

$$D = K\lambda \; / \; \beta Cos \; \theta \tag{1}$$

The crystals' average size was estimated to be 24.22 nm.

FESEM/EDX analysis

The surface morphology of CT-CS nanoparticles was assessed by FE-SEM (Fig. 3a), which demonstrated their regular, spherical form and minimal aggregation. Using energy dispersive X-ray analysis (EDX), the elemental makeup of CT-CS nanoparticles was determined. Elements of O, Si, Ca, and Ti are clearly present in CT-CS nanoparticles (Fig. 3b). Based on the CT-Cs nanoparticle size distribution histogram (Fig. 3c), the average particle size of nanoparticles is estimated to be around 45.76 nm.

One of the main causes of nanoparticle aggregation is high temperatures (950 °C) during calcination, a process in which a material is heated to high temperatures. This can cause single nanoparticles to cluster and bond, forming larger objects. This aggregation process is primarily caused by surface attractive interactions, such as Van der Waals forces. In nanoparticles, which have a small particle size and high surface area-to-volume ratio, Van der Waals interactions (weak attractive forces between molecules) are more significant than electrostatic repulsion forces. As a result, the average crystalline size and particle size may differ.

Optimization using response surface methodology

The mechanical properties of the EP/PVAc/CT-CS/CF nanocomposite were measured using by a tensile test machine, and the results are shown in Table 2. Additionally, the result of stress, strain, and area analysis of variance (ANOVA) results indicate that a p-value of less than 0.05 suggests that the models are significant, while lack of fit is not significant that showed the models are well-fitted to the experiment. Additionally, the area, stress, and strain regression coefficients (R^2) are, respectively, 0.9417, 0.8775, and 0.8496. Obtained R^2 from ANOVA indicated a high correlation between experimental and predicted values. The following is the final equation in terms of actual factors that was derived.

The R^2 value for strain is lower than that for stress and area, indicating that the correlation between experimental and theoretical data is weaker for strain compared to stress and area. According to the 3D graphs, stress and area exhibit linear behavior, while strain demonstrates nonlinear behavior, resulting in a lower R^2 value for strain. Additionally, the complex interactions between dependent parameters, such as PVAc, CF, and nanoparticles, may not be fully captured

Table 3. The optimum percentage weight of A, B, and C in the fabrication of EP/PVAc/CTO-CS/CF nanocomposites and the results of their validation experiment.

The Optimum nanocomposite	optimum percentage weight			Response	
	A (NPs)	B(CF)	C(PVAc)	Predicted	Experimental
Maximum Stress (MPa)	1.196	0.797	5.189	32.171	43.19
Maximum Strain (%)	0.304	0.763	4.717	8.460	7.69
Maximum Area (J)	0.304	0.797	5.189	577.984	433.91

Table 4. Comparison in improving the mechanical properties of optimal specimens compared to pure epoxy and EP/PVAc.

Response (%)	Stress		Strain		Area	
	EP	EP/PVAc	EP	EP/PVAc	EP	EP/PVAc
Maximum Stress	236.68	188.89	-68.78	-67.96	-60.13	-60.23
Maximum Strain	150.15	114.51	-76.40	-75.79	-65.33	-65.42
Maximum Area	159.43	122.47	-76.07	-75.45	-65.68	-67.77

by the current model. Residual plots from the Design Expert software confirm that the data dispersion around the 45-degree line is slightly wider for strain than for stress and area, further contributing to the lower R² value for strain.

$$Stress=3.23639+1.60458A+23.72668B+1.56060C \quad (2)$$

$$Strain=6.39715-3.90800A+6.34551B+0.197654C-3.90323AB+0.037712AC+0.395989BC+3.17116A^2-4.18990B^2-0.042806C^2 \quad (3)$$

$$Area=221.25-6.52A+122B+47.90C+10.1AB-42.94AC+30.50BC+55.08A^2+39.13B^2+22.67C^2 \quad (4)$$

The optimum percentage weight of CF, PVAc, and NPs for the fabrication of nanocomposites and the comparison between predicted data and experimental values are shown in Table 3. The results show a slight discrepancy between the experimental and theoretical outcomes.

Design Expert software is divided into two main sections: numerical and optimization. Once 20 experiments have been designed and their
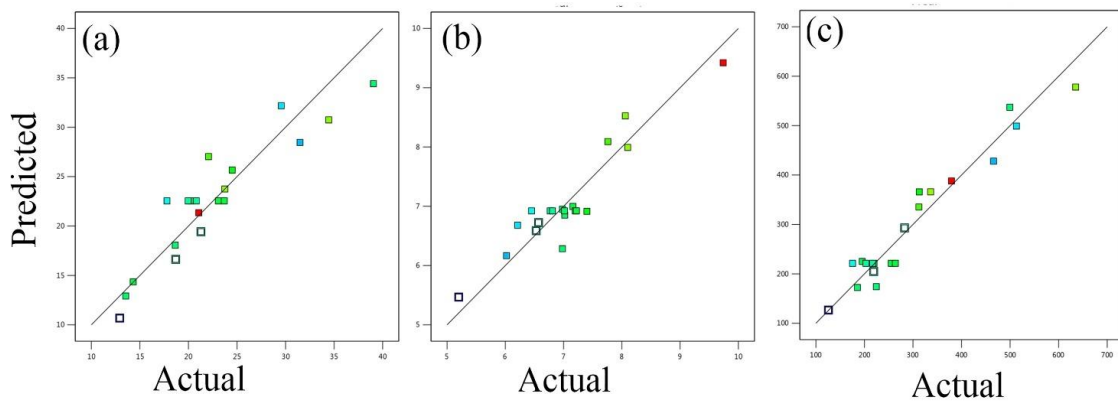
Fig. 4. Plots of predicted versus actual values for stress, strain, area, module, and yield (a-e).
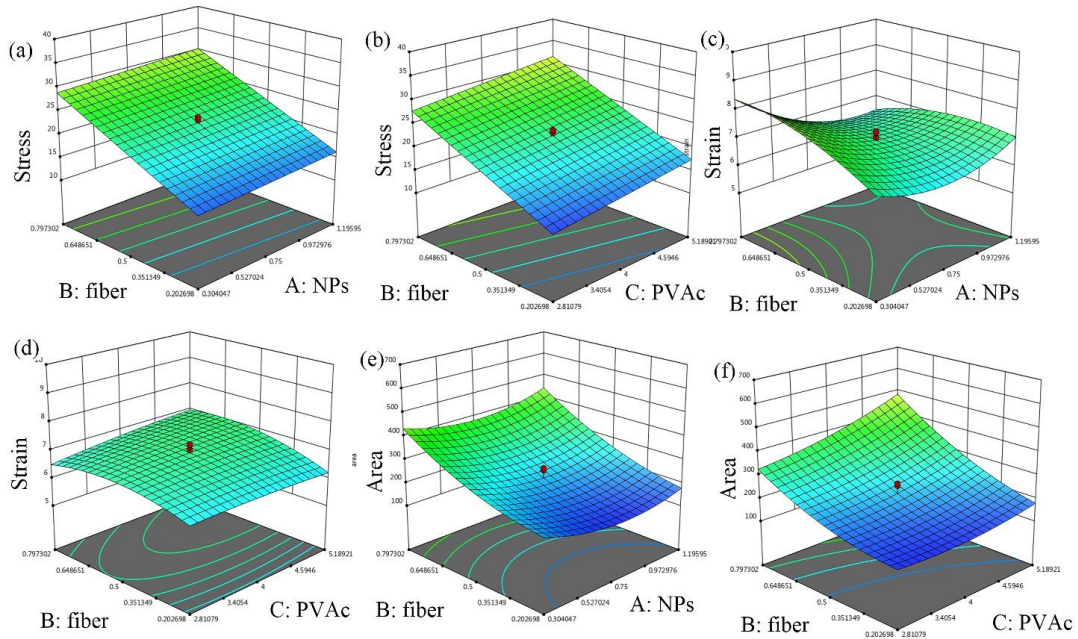
Fig. 5. 3D graphs of the optimal (a, b) maximum stress, (c, d) maximum strain (e, f) maximum area of EP/ PVAc/CT-CS/CF nanocomposites.

responses entered into the software, an ANOVA analysis can be performed. This allows the software to carry out optimization and determine the percentage weight of each variable. For example, to identify the percentage weight for the maximum stress sample, the stress is set to its maximum value while keeping other parameters within their respective ranges. A similar approach is used for other parameters, such as strain and area. In these cases, strain and area are individually defined as the maximum parameters, while the other variables remain within their designated ranges. The software then calculates the weight percentages for each optimal sample.

The comparison between the pure epoxy and EP/PVAc samples compared to the optimal samples shows an increase of 236.68% and 188.89% in the optimal maximum stress nancomposite, respectively. For other the optimum nanocomposites (maximum strain and maximum area), a declining trend is observed (Table 4).

The correlation between the actual and predicted responses for stress, strain, and area,

respectively, is displayed in Figs. 4(a–c). According to the figure, there was a good correlation between the actual and predicted response values.

Fig. 5 displays 3D graphs depicting stress, strain, and area, respectively. As the amounts of nanoparticles and PVAc increased, the stress response showed a slight incline and Demonstrated a linear trend. The addition of fiber had a significant impact on the stress value which can be seen in a noticeable upward trend (Figs. 5a and 5b).

The effect of increasing nanoparticles and fiber on strain did not follow a linear inclination. The value of strain decreased at first when the ratio of nanoparticles was increased to 0.75 weight percent; after that, it gradually increased. A gradual decrease in strain value is observed after an initial increase with the increase in the weight percentage of fiber. No change in the strain response was observed when varying the weight percentage of PVAc (Figs. 5c and 5d).

The tendency in changes in the area's response are nonlinear, similar to the strain. The effect of fiber on increasing area is more significant than
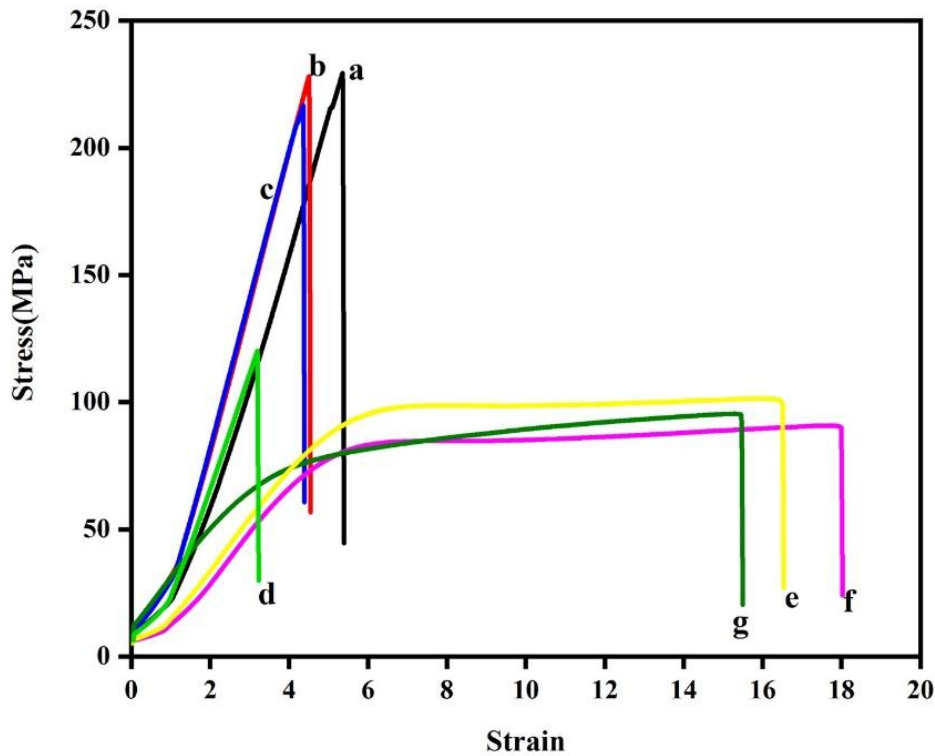
Fig. 6. Stress-strain plots of the optimal (a) maximum stress, (b) maximum strain, (c) maximum area nanocomposites, (d) EP/CF, (e) EP, (f) EP/NPs, and (g) EP/PVAc nanocomposites.

that of PVAc and nanoparticles. No discernible difference in the area's response was observed when the weight percentage of PVAc (4 weight%) was increased. A modest decrease was observing after adding the nanoparticles at the 0.75 weight percentage, followed by a small increase (Figs. 5e and 5f).

The stress-strain charts for the EP, EP/PVAc, EP/CT-CS, EP/CF, and the optimum nanocomposites (maximum stress, maximum strain, and maximum area) are displayed in Fig. 6. The top section of Fig. 6 illustrates how the optimum samples' mechanical qualities were better than those of the other samples. Among the parameters, carbon fiber is the most effective parameter for increasing stress, while other parameters (CT-CS nanoparticles and PVAc) have a low impact on improving stress.

This suggests that CF has a significant positive impact on certain parameters, such as stress, with an increase of 236.7%, while it has a negative effect on strain. Based on SEM images (Fig. 9), the displacement of fibers in the epoxy matrix is lower in the stress sample compared to the strain sample. This indicates that the interfacial bonding between EP and CF is stronger in the stress sample. The interface between the matrix and modified CF plays a crucial and promising role in enhancing the mechanical properties of the nanocomposites. Additionally, the high modulus of CF (200 to 500 GPa) and its specific tensile strengths (3 to 7 GPa) contribute to the stiffness of the nanocomposite, further increasing its mechanical properties compared to the strain sample. The stress-strain curve also shows that samples containing CF exhibit an increase in stress and the area under the curve, resulting in
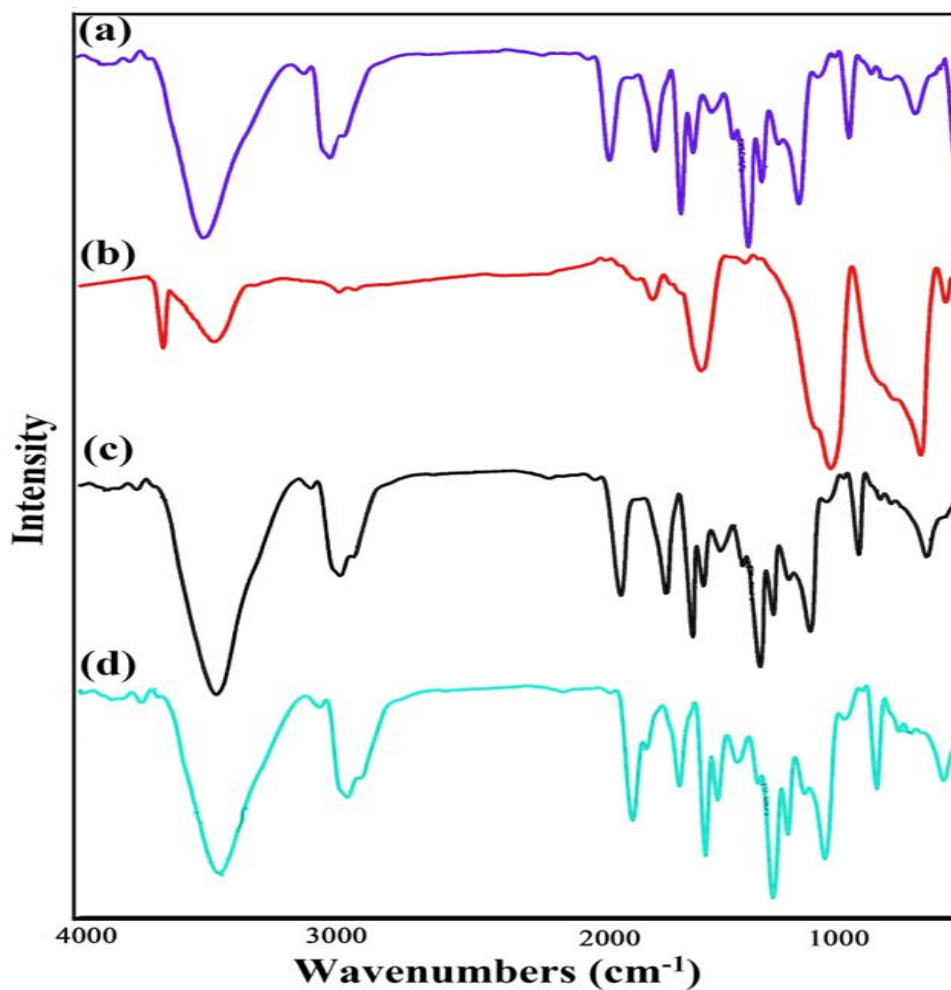
Fig. 7. FT-IR of EP (a), CT-CS nanoparticles (b), EP/CT-CS (c), and EP/ PVAc/CT-CS (d).

a harder nanocomposite with reduced strain or elongation. Finally, the combination of CF, PVAc, and nanoparticles creates a synergistic effect that significantly enhances the stress response compared to the strain sample.

Comparing the mechanical properties of EP/PVAc, EP/CF, and EP/CT-CS nanocomposites with pure epoxy resin with the same percentages of the optimal maximum stress sample shows their stress responses increased by 16.37%, 50%, and 7.06%, respectively. The effect of PVAc and NPs on improving stress are less significant than those of CF in enhancing the stress response. Furthermore, these three components complement each other well, producing a synergistic effect that raises the overall stress in epoxy resin by 236.7%.

Nanocomposites characterization
XRD analysis
The XRD pattern of EP/PVAc/CT-CS/CF

nanocomposites indicates an amorphous structure due to the low presence of nanoparticles compared to the EP matrix (Figures 1b and 1c).

FTIR analysis
The FT-IR spectra of EP, CT-CS nanoparticles, EP/CT-CS, and EP/PVAc/CT-CS nanocomposites are displayed in Fig. 7, in that order. Peaks at 1610, 1509, and 1458 cm^{-1} indicate the C=C vibrations of the aromatic ring in epoxy resin. The peak at 1738 cm^{-1} is believed to the C=O vibration of the carbonyl group in EP. The epoxy resin contains oxirane and hydrogen-bonded C–OH groups, as indicated by the peaks at 1118 and 827 cm^{-1} [19]. The CT-CS nanoparticle has a strong peak at 925, 563, and 451 cm^{-1}, which are indicative of the Ca-O-Si and Ca-O-Ti bonds, respectively (Fig. 7b).

The significant peaks of epoxy are also observed in EP/CT-CS and EP/PVAc (Figs. 7c and 7d). The FT-IR spectra of the optimal nanocomposites are
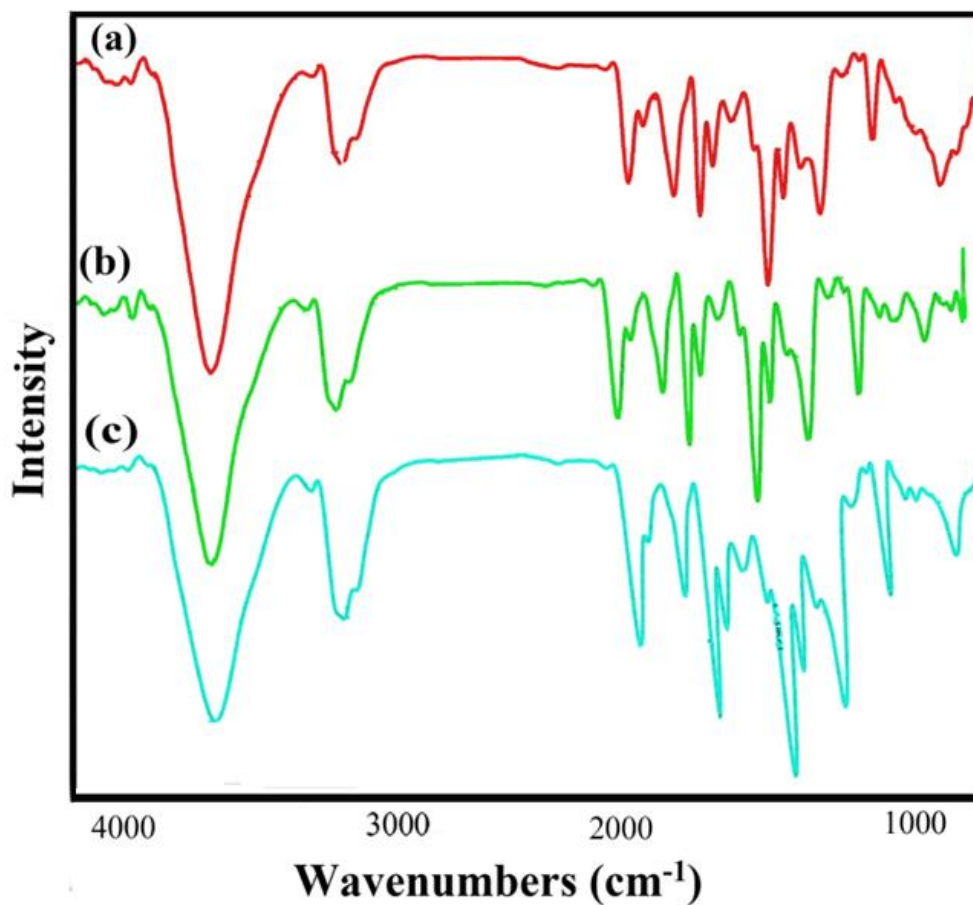
Fig. 8. FT-IR spectrum of the optimal nanocomposite with (a) maximum stress, (b) maximum strain, and (c) maximum area.

presented in Fig. 8. They have certain peaks that are very similar to those of pure epoxy [35-37].

FESEM/EDX analysis

The cross-sectional SEM image of EP/PVAc is displayed in Fig. 9a, revealing a smooth surface with scattered air bubbles. Figs. 9c and 9e present SEM images of the optimal maximum strain and maximum stress nanocomposites, respectively.

The uniformity of the surface suggests a high level of nanoparticle dispersion, resulting in reduced air bubbles. Furthermore, cross-sectional SEM images demonstrate fiber displacement and extraction in maximum strain sample is remarkable than that of stress maximum sample, with a CF diameter of approximately 7 μm. The EDAX spectrum of EP/PVAc is represented in Fig. 9b, while the analysis for the optimal maximum strain and maximum
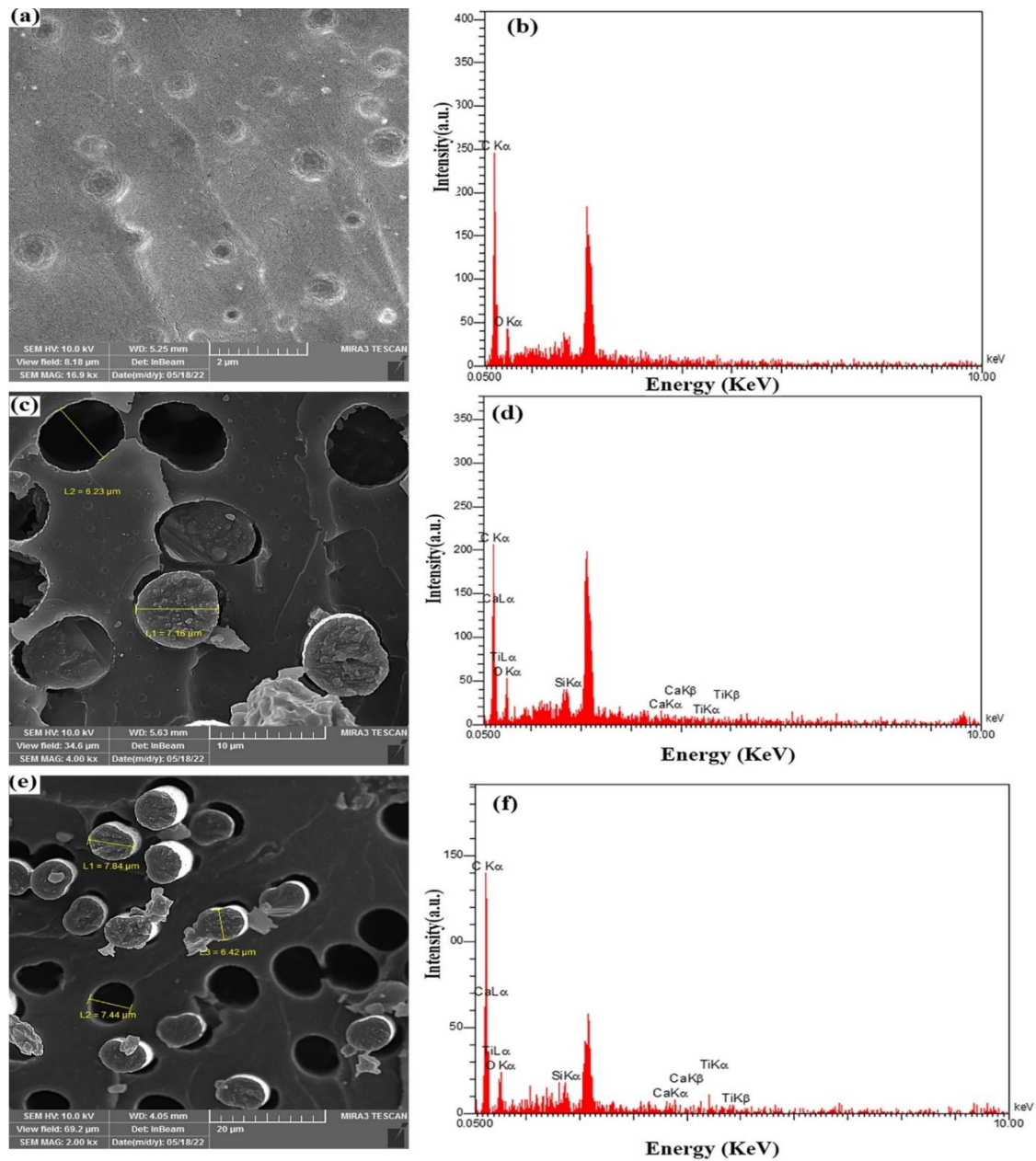
Fig. 9. SEM image and EDX of (a, b) EP/PVAc, the optimal nanocomposite with (c, d) maximum strain, and (e, f) maximum stress.

stress nanocomposites are shown in Figs. 9d and 9f, respectively. These samples clearly differ in elementally from EP/PVAc, indicating the presence of nanoparticles.

TGA analysis

Fig. 10 displays the TGA graph for the optimal samples and pure EP. There are two stages of mass loss, according to the TGA curves. The initial phase, which occurs between 100 and 300 °C, is caused by the samples' moisture loss. The second stage relates to the breakdown of the epoxy resin and occurs between 300 and 500 °C. The first step refers to the burning of the sample and the second one is concerned with the decomposition of a layer of char.

This stage is the main target of degradation due to the high concentration of epoxy resin.

The weight loss in the samples is shown in Table 5. Strain samples have the highest concentration of EP resin but the lowest concentrations of PVAc, CF, and nanoparticles. However, EP resin has a thermal stability of X between 300 and 600 °C, which is lower than CF and nanoparticles. The strain sample degraded earlier than the other samples due to its higher concentration of EP resin. The interfacial interaction between the fiber and matrix and the weak interfacial bonding of the heat-resistant substance CF affects the performance of nanocomposites, causing decreased heat stability and accelerating weight loss in this sample.

In contrast, the stress sample exhibits higher thermal stability than the other samples, which can be attributed to the strong interfacial bonding between the EP matrix and CF. The inclusion of
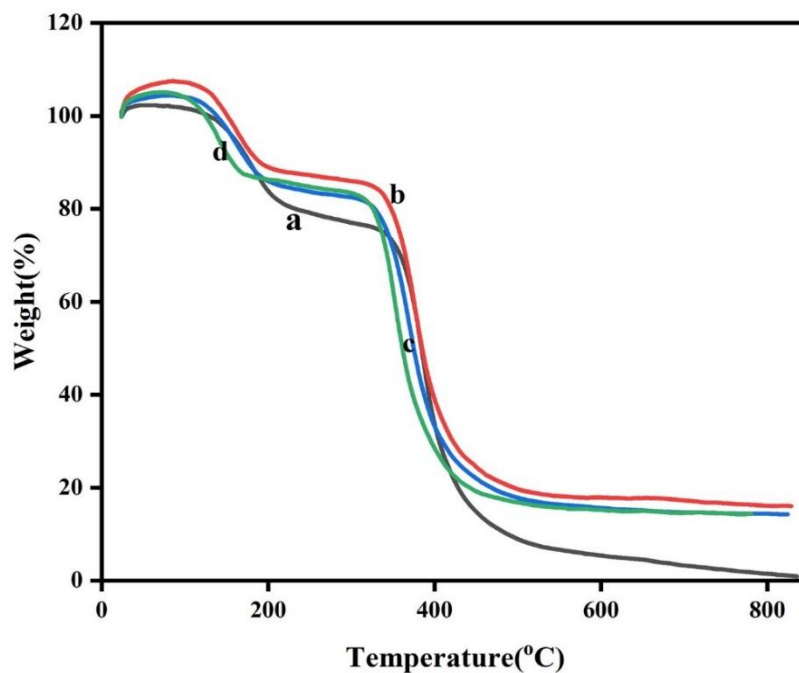
Fig. 10. TGA curve of the optimal nanocomposite with (a) maximum strain, (b) maximum area, (c) maximum stress, and (d) EP.

Table 5. Degradation percentage of EP and the optimum nanocomposite in different temperature.

samples	%Degradation in 100-300°C	%Degradation in 300-600°C	% Remaining
EP	19.77	65.33	14.9
maximum Stress	20.98	64.17	14.85
maximum Strain	24.73	70.95	4.32
maximum Area	19.71	64.26	16.03

CF, PVAc, and (CT-CS) nanoparticles leads to the formation of heterogeneous interfaces within the composite matrix. As previously mentioned, CF acts as a heat barrier, while PVAc and nanoparticles can modify the thermal properties of the matrix, potentially creating weak spots that initiate earlier decomposition.

The degradation temperature of epoxy resin in an argon-containing atmosphere starts at 320 °C and ends at 460 °C. PVAc degrades in two stages: in the first stage (240–310 °C), its thermal degradation produces a high proportion of acetic acid. Additionally, some aromatic hydrocarbons were detected. Simultaneous decomposition of PVAc and the epoxy matrix can result in overlapping degradation stages, making it challenging to distinguish their contributions. More important than all of these factors, instrumental problems and errors during the analysis have led to unpredictable errors in the process of analyzing the results [38, 39].

CONCLUSION

The EP/PVAc/CT-CS/CF nanocomposite was prepared using a direct mixing method, and its chemical and mechanical properties were studied. The RSM/CCD approach was employed to optimize the weight percentages of NPs, PVAc, and CF to improve the mechanical properties of stress, strain, and area. Significant mechanical properties such as stress, strain, and area was measured using the tensile test apparatus. Compared to NPs and PVAc, carbon fiber has a more noticeable effect on improving the response. The effect of the aforementioned parameters on the improvement of strain and area response were less than those of stress. These results indicate a significant increase in the response to stress compared to strain and area. Specifically, there was an increase of 236.68% and 188.89% in the response to stress when compared to EP and EP/PVAc. The changes in stress, strain, and area between pure epoxy and fiber-reinforced epoxy are 50%, -78%, and -82.89%, respectively.

ACKNOWLEDGMENTS

CONFLICT OF INTEREST

The authors declare that there is no conflict of interests regarding the publication of this manuscript.

REFERENCES

1. Altin Karataş M, Gökkaya H. A review on machinability of carbon fiber reinforced polymer (CFRP) and glass fiber reinforced polymer (GFRP) composite materials. Defence Technology. 2018;14(4):318-326.
2. Karnati SR, Agbo P, Zhang L. Applications of silica nanoparticles in glass/carbon fiber-reinforced epoxy nanocomposite. Composites Communications. 2020;17:32-41.
3. Jin F-L, Li X, Park S-J. Synthesis and application of epoxy resins: A review. Journal of Industrial and Engineering Chemistry. 2015;29:1-11.
4. Unnikrishnan KP, Thachil ET. Toughening of epoxy resins. Designed Monomers and Polymers. 2006;9(2):129-152.
5. Zotti A, Zuppolini S, Zarrelli M, Borriello A. Fracture Toughening Mechanisms in Epoxy Adhesives. Adhesives - Applications and Properties: InTech; 2016.
6. Ghasemi-Kahrizsangi A, Neshati J, Shariatpanahi H, Akbarinezhad E. Effect of SDS modification of carbon black nanoparticles on corrosion protection behavior of epoxy nanocomposite coatings. Polym Bull. 2015;72(9):2297-2310.
7. Choi YY, Lee SH, Ryu SH. Effect of silane functionalization of montmorillonite on epoxy/montmorillonite nanocomposite. Polym Bull. 2009;63(1):47-55.
8. Qiao Y, Wang P, Xue X, Liu M, Xu S. Enhancing the dynamic temperature stability of epoxy with graphene oxide. Mech Mater. 2020;150:103593.
9. Vijayan P P, Tanvir A, Mrlik M, Urbanek M, Al-Maadeed M. TiO$_2$/Halloysite hybrid filler reinforced epoxy nanocomposites. Polym Compos. 2018;39(S4).
10. Annappa AR, Basavarajappa S, Davim JP. Effect of organoclays on mechanical properties of glass fiber-reinforced epoxy nanocomposite. Polym Bull. 2021;79(7):5085-5103.
11. Wu J, Yu K, Qian K, Jia Y. One step fabrication of multi-walled carbon nanotubes/graphene nanoplatelets hybrid materials with excellent mechanical property. Fibers and Polymers. 2015;16(7):1540-1546.
12. Xia X, Liu Y, Zhang J, Luo J, Weng GJ. Tailoring electromagnetic interference shielding effectiveness of SiO$_2$-decorated MWCNT/polymer nanocomposites. Mech Mater. 2024;191:104949.
13. Dehrooyeh S, Vaseghi M, Sohrabian M, Sameezadeh M. Glass fiber/Carbon nanotube/Epoxy hybrid composites: Achieving superior mechanical properties. Mech Mater. 2021;161:104025.
14. Sarafrazi M, Hamadanian M, Ghasemi AR. Optimize epoxy matrix with RSM/CCD method and influence of multi-wall carbon nanotube on mechanical properties of epoxy/polyurethane. Mech Mater. 2019;138:103154.
15. Xie Y, Liu W, Liang L, Liu C, Yang M, Shi H, et al. Incorporation of silica network and modified graphene oxide into epoxy resin for improving thermal and anticorrosion properties. J Appl Polym Sci. 2020;137(45).
16. Zeng S, Shen M, Xue Y, Zheng Y, Zhang K, Han Y, et al. Controllable mechanical properties of epoxy composites by incorporating self-assembled carbon nanotube–montmorillonite. Composites Part B: Engineering. 2019;164:368-376.
17. Shabani N, Hamadanian M, Ghasemi AR, Sarafrazi M.

Physicochemical and Mechanical Properties of Epoxy/ Polyurethane/Nickel Manganite Nanocomposite: A Response Surface Methodology/Central Composite Designs Study. Journal of Inorganic and Organometallic Polymers and Materials. 2018;28(6):2689-2700.

18. Abbasi A, Hamadanian M, Salavati-Niasari M, Mazhari MP. Hydrothermal synthesis, characterization and photodegradation of organic pollutants of $CoCr_2O_4$/Ag nanostructure and thermal stability of epoxy acrylate nanocomposite. Adv Powder Technol. 2017;28(10):2756-2765.

19. Ashrafi M, Hamadanian M, Ghasemi AR, Kashi FJ. Improvement mechanical and antibacterial properties of epoxy by polyethylene glycol and Ag/CuO nanoparticles. Polym Compos. 2019;40(9):3393-3401.

20. Cui HW, Du GB. Preparation and characterization of exfoliated nanocomposite of polyvinyl acetate and organic montmorillonite. Adv Polym Tech. 2011;31(2):130-140.

21. Kramár S, Trcala M, Chitbanyong K, Král P, Puangsin B. Basalt-Fiber-Reinforced Polyvinyl Acetate Resin: A Coating for Ductile Plywood Panels. Materials (Basel, Switzerland). 2019;13(1):49.

22. Lapprand A, Arribas C, Salom C, Masegosa RM, Prolongo MG. Epoxy resins modified with poly(vinyl acetate). J Mater Process Technol. 2003;143-144:827-831.

23. Moya R, Rodríguez-Zúñiga A, Vega-Baudrit J, Álvarez V. Effects of adding nano-clay (montmorillonite) on performance of polyvinyl acetate (PVAc) and urea-formaldehyde (UF) adhesives in Carapa guianensis, a tropical species. Int J Adhes Adhes. 2015;59:62-70.

24. Mohanty A, Srivastava VK. Effect of alumina nanoparticles on the enhancement of impact and flexural properties of the short glass/carbon fiber reinforced epoxy based composites. Fibers and Polymers. 2015;16(1):188-195.

25. Nayak RK, Dash A, Ray BC. Effect of Epoxy Modifiers (Al_2O_3/ SiO_2/TiO_2) on Mechanical Performance of epoxy/glass Fiber Hybrid Composites. Procedia Materials Science. 2014;6:1359-1364.

26. Rahmani H, Eslami-Farsani R, Ebrahimnezhad-Khaljiri H. High Velocity Impact Response of Aluminum- Carbon Fibers-Epoxy Laminated Composites Toughened by Nano Silica and Zirconia. Fibers and Polymers. 2020;21(1):170-178.

27. Kolosov AE. Preparation of Reactoplastic Nano-Modified Polymer Composites. Part 5. Advantages of Using Nano-Modified Structural Carbon-Fiber Composites (A Review)*. Chemical and Petroleum Engineering. 2017;52(9-10):721-725.

28. Bisht A, Dasgupta K, Lahiri D. Investigating the role of 3D network of carbon nanofillers in improving the mechanical properties of carbon fiber epoxy laminated composite. Composites Part A: Applied Science and Manufacturing. 2019;126:105601.

29. Dong J, Jia C, Wang M, Fang X, Wei H, Xie H, et al. Improved mechanical properties of carbon fiber-reinforced epoxy composites by growing carbon black on carbon fiber surface. Composites Science and Technology. 2017;149:75-80.

30. Khan SU, Munir A, Hussain R, Kim J-K. Fatigue damage behaviors of carbon fiber-reinforced epoxy composites containing nanoclay. Composites Science and Technology. 2010;70(14):2077-2085.

31. Khan ZI, Arsad A, Mohamad Z, Habib U, Zaini MAA. Comparative study on the enhancement of thermo-mechanical properties of carbon fiber and glass fiber reinforced epoxy composites. Materials Today: Proceedings. 2021;39:956-958.

32. Vedrtnam A. Novel method for improving fatigue behavior of carbon fiber reinforced epoxy composite. Composites Part B: Engineering. 2019;157:305-321.

33. Wu C, Ramaswamy Y, Soeparto A, Zreiqat H. Incorporation of titanium into calcium silicate improved their chemical stability and biological properties. Journal of Biomedical Materials Research Part A. 2007;86A(2):402-410.

34. Rafiee-Pour H-A, Hamadanian M, Koushali SK. Nanocrystalline TiO_2 films containing sulfur and gold: Synthesis, characterization and application to immobilize and direct electrochemistry of cytochrome c. Appl Surf Sci. 2016;363:604-612.

35. Balbinot GdS, Leitune VCB, Nunes JS, Visioli F, Collares FM. Synthesis of sol–gel derived calcium silicate particles and development of a bioactive endodontic cement. Dent Mater. 2020;36(1):135-144.

36. Füllbrandt M, Purohit PJ, Schönhals A. Combined FTIR and Dielectric Investigation of Poly(vinyl acetate) Adsorbed on Silica Particles. Macromolecules. 2013;46(11):4626-4632.

37. Meiszterics A, Rosta L, Peterlik H, Rohonczy J, Kubuki S, Henits P, et al. Structural Characterization of Gel-Derived Calcium Silicate Systems. The Journal of Physical Chemistry A. 2010;114(38):10403-10411.

38. Costa L, Avataneo M, Bracco P, Brunella V. Char formation in polyvinyl polymers I. Polyvinyl acetate. Polymer Degradation and Stability. 2002;77(3):503-510.

39. Jiang G, Pickering SJ, Walker GS, Bowering N, Wong KH, Rudd CD. Soft ionisation analysis of evolved gas for oxidative decomposition of an epoxy resin/carbon fibre composite. Thermochim Acta. 2007;454(2):109-115.